EBioMedicine 62 (2020) 103096

Contents lists available at ScienceDirect

EBioMedicine

journal homepage: www.elsevier.com/locate/ebiom

Research paper

Computed tomography-adjusted fistula risk score for predicting clinically relevant postoperative pancreatic fistula after pancreatoduodenectomy: Training and external validation of model upgrade

Yu Shi[a,1,*], Feng Gao[b,1], Yafei Qi[c], Hong Lu[d], Fulu Ai[e], Yang Hou[a], Chang Liu[a], Youli Xu[a], Xianyi Zhang[a], Xiaoli Cai[a]

[a] Department of Radiology, Shengjing Hospital of China Medical University, No. 36, Sanhao Street, Heping District, Shenyang 110004, China
[b] Department of Pancreato-thyroidic Surgery, Shengjing Hospital of China Medical University, Shenyang, China
[c] Department of Pathology, Shengjing Hospital of China Medical University, Shenyang, China
[d] Department of Radiology, Tianjin Medical University Cancer Institute and Hospital, National Clinical Research Center of Cancer, Key Laboratory of Cancer Prevention and Therapy, Tianjin, P R China
[e] Department of General Surgery, Cancer Hospital of China Medical University, Liaoning Cancer Hospital and Institute, Shenyang, Liaoning Province 110042, P R China

ARTICLE INFO

Article History:
Received 15 June 2020
Revised 12 October 2020
Accepted 13 October 2020
Available online xxx

Keywords:
Postoperative pancreatic fistula
Pancreaticoduodenectomy
Computed tomography
Risk prediction

ABSTRACT

Background: To develop a modified Fistula Risk Score (FRS) for predicting clinically relevant postoperative pancreatic fistula (CR-POPF) after pancreatoduodenectomy (PD) based on both FRS and contrast-enhanced computed tomography (CE-CT).
Methods: In this multicenter retrospective analysis, we focused on 990 consecutive patients with pancreatoduodenectomy performed at four institutions between 2009 and 2019. The enhanced CT-FRS model initially targeted 26 pre- and intraoperative factors, including CT descriptors, FRS elements and clinical factors, using LASSO-penalized multivariable logistic regression for predicting CR-POPF events in discovery (n = 718) and externally validated (n = 272) datasets. Probabilities generated were further correlated with histologic features of pancreatic stumps in 356 patients. C-indices were analyzed to compare the predictive potential between the original FRS and the CT-FRS.
Findings: CR-POPF developed in 112 (15.6%) and 36 (13.2%) patients in discovery and validation datasets, respectively. The final CT-FRS construct, incorporating remnant pancreatic volume (RPV), stump area, fat and atrophy scores by CT, and main pancreatic duct size, offered significantly greater overall predictability than the original FRS in discovery (C-index: 0.825 vs 0.794; p = 0.04) and validation (0.807 vs 0.741; p = 0.05) cohorts. Importantly, it outperformed the FRS in patients at moderate risk levels (FRS: 3–6), showing remarkably improved C-indices (discovery: 0.729 vs 0.626 [$p<0.001$], validation: 0.722 vs 0.573 [p = 0.006]). CT-FRS probabilities increased in conjunction with less extensive pancreatic fibrosis ($p<0.001$), ample glandular acini ($p<0.001$), and advanced lipomatosis ($p<0.001$).
Interpretation: The enhanced CT-FRS performed significantly better than the original FRS in predicting CR-POPF occurrences after PD, especially at moderate FRS levels.

1. Introduction

Pancreatoduodenectomy (PD) is one of the most technically challenging operations in the surgical field, and postoperative pancreatic fistula (POPF) is considered the most serious major procedural complication [1–3]. Despite continued efforts over time to devise or improve pancreaticoenteric anastomotic techniques, clinically-relevant POPF (CR-POPF) regularly occurs in ~11–15% of patients [4-9]. Not only is hospitalization prolonged and the cost of medical treatment increased, but there is also a potential for abscesses of

Abbreviations: PD, pancreatoduodenectomy; POPF, postoperative pancreatic fistula; CR-POPF, clinically-relevant postoperative pancreatic fistula; ISGPS, International Study Group of Pancreatic Surgeons; FRS, Fistula Risk Score; MPD, main pancreatic duct; BMI, body mass index; CE-CT, contrast-enhanced computed tomography; NCCN, National Comprehensive Cancer Network; PACS, picture archiving and communication system; VFA, visceral fat area; RPV, remnant pancreatic volume; PJ, pancreaticojejunostomy; PG, pancreaticogastrostomy; ISGPF, International Study Group of Pancreatic Fistula; HE, hematoxylin and eosin; ICCs, Intraclass correlation coefficients; LASSO, least absolute shrinkage and selection operator

* Corresponding author.
E-mail address: 18940259980@163.com (Y. Shi).
[1] Yu Shi and Feng Gao contributed equally to the manuscript as first co-authors.

https://doi.org/10.1016/j.ebiom.2020.103096

Research in context

Evidence before this study

We systematically searched PubMed, without date restriction or limitation to English language publications, for research articles with the following terms: (postoperative pancreatic fistula OR POPF OR pancreatic fistula) AND (predictor OR predictive OR prediction) AND (pancreatic surgery OR Pancreatoduodenectomy OR pancreatic operation). Previous studies showed that there were dozens of intraoperative or preoperative factors affecting the presence of postoperative pancreatic fistula, including main pancreatic duct [MPD] size, pancreatic texture, definitive pathology, and intraoperative blood loss, body mass index, and morphological measurements of the pancreatic stump or the pancreatic remnant parenchyma. Among these methods, the Fistula Risk Score (FRS) was reported as a well-established and externally validated scale for predicting the occurrences of clinically relevant POPF (CR-POPF). However, it needs intraoperative evaluations, and ~50% patients are at the gray zone with moderate risk (FRS: 3−6), warranting more specific, accurate and preoperative predictors. The published computed tomography (CT) features included either the morphological measurements (pancreatic thickness/width, stump area, remnant volume, duct size) or the subjective evaluations (pancreatic atrophy) via radiologist's classifications. Until now, these studies used single CT predictors. A robust CT-based predictive model had not been fully developed or externally validated in a large sample size, nor had any incremental adjustment of clinical FRS predictions been pursued in previously published papers.

Added value of this study

We developed and externally validated the first CT-FRS model as a modification of the established original FRS. Our CT-FRS model is based upon 5 aforementioned risk factors for CR-POPF, which were originally discerned from a multivariate analysis of 26 preoperative and intraoperative factors. By adding pancreatic CE-CT to the FRS framework, the overall predictive performance levels (C-indices) of 0.80−0.85 were achieved in discovery and external validation cohorts. The CT-FRS model substantially improved FRS predictive capability, specifically in the challenging patients at moderate levels of risk (FRS: 3−6).

Implications of all the available evidence

Our findings, together with existing evidence, served to identify patients who benefitted the most from preoperative CT imaging features in predicting the development of CR-POPF after pancreatoduodenectomy. Based on our CR-FRS model, an open-source online calculator is offered for the estimated probability of CR-POPF risk for clinicians. This model can be used to stratify patients into distinct clinical-outcome, enabling new insights into diagnosis and treatment of CR-POPF occurrence. Future research should focus on the incorporation of CT-FRS into surgical planning for optimal decision-making and patient care.

catastrophic nature or subsequent lethal hemorrhage, heightening morbidity/mortality rates [10]. Sensitive predictors that identify patients at high risk of CR-POPF would greatly assist surgical specialists in managing pancreatic fistulas, focusing on timely prevention in high-risk patients and sparing low-risk patients from overly zealous therapeutics [11].

POPF results from localized leakage of pancreatic juice at the pancreaticoenteric anastomotic stump after PD [11]. As defined by the International Study Group of Pancreatic Surgeons (ISGPS) in 2005 and revised in 2016 [8,12], a POPF that impacts postoperative clinical management, graded B or C, is considered a CR-POPF [8]. The Fistula Risk Score (FRS) incorporates four predictive parameters (main pancreatic duct [MPD] size, pancreatic texture, definitive pathology, and intraoperative blood loss) and is a standard, validated 10-point grading scale used to predict occurrences of CR-POPF [13-15]. The more recently established alternative FRS (a-FRS) instead addresses MPD, pancreatic texture, and body mass index (BMI) [16], ignoring blood loss and pathology. However, it still relies on intraoperative evaluations, and ~50% patients are in a gray zone of moderate risk (FRS: 3−6) [14-17], so preoperative predictors of greater accuracy and specificity are needed. Moreover, beyond MPD diameter (included in both FRS and a-FRS), morphologic risk factors at pancreatic stump [18-20] (eg, pancreatic thickness, stump area) that directly impact anastomotic failure have been otherwise discounted. Such factors are readily assessable in standard-of-care contrast-enhanced computed tomography (CE-CT) images.

Until now, a robust CT-based predictive model had not been fully developed or externally validated in a large sampling, nor had any incremental adjustments of clinical FRS predictions been pursued. Our intent was to: 1) develop and externally validate a new predictive model combining CE-CT with clinical FRS items in predicting CR-POPF, 2) compare performances of the optimized CT-FRS model and FRS or a-FRS reference methods in various risk zones, and 3) correlate resultant probabilities with underlying histologic changes (fibrosis, glandular atrophy, and lipomatosis) at anastomotic stump.

2. Materials and methods

2.1. Ethics statement

This was a multicenter, multicohort retrospective study involving four academic institutions. The protocol adhered to ethical standards of the 1964 Helsinki Declaration, including its later amendments, and was approved by Institutional Review Boards at Shengjing Hospital of China Medical University, Liaoning Cancer Hospital and Institute, Tianjin Medical University Cancer Institute and Hospital and Guangdong General Hospital (IRB number 2016PS191K, 2017PS236K and 2018PS298K (T1)). These patients were from three main territories of China (Northeast, North and South China) and includes rural, urban, and suburban populations. Informed consent was waived across all cohorts.

2.2. Study population

TRIPOD guidelines for multivariable prediction models were applied during design [21], validation, and reporting of the clinical prediction model. Each patient with PD was enrolled between January 2009 and November 2019 (Fig. 1). By design, the discovery dataset from two independent institutions (Shengjing Hospital of China Medical University [Shenyang, China], n = 562, January 2009 to August 2019; Liaoning Cancer Hospital and Institute, [Shenyang, China], n = 156, January 2014 to August 2019). Of these patients (n = 718), roughly one-half (n = 356) were chronicled in a prospectively maintained database from Shengjing Hospital (January 2016 to August 2019), each having histologic evaluation of the anastomotic stump area. For external validation, data on patient outcomes (n = 272) at another two institutions (Tianjin Medical University Cancer Institute and Hospital [Tianjing, China], n = 212, January 2010 to November 2019; Guangdong General Hospital [Guangdong, China], n = 60, January 2011 to August 2015) were retrospectively retrieved from medical archives.

2.3. Preoperative CT imaging and evaluations

All patients underwent preoperative multiphasic scans within 4 weeks of surgery with at least two contrast-enhanced phases and one

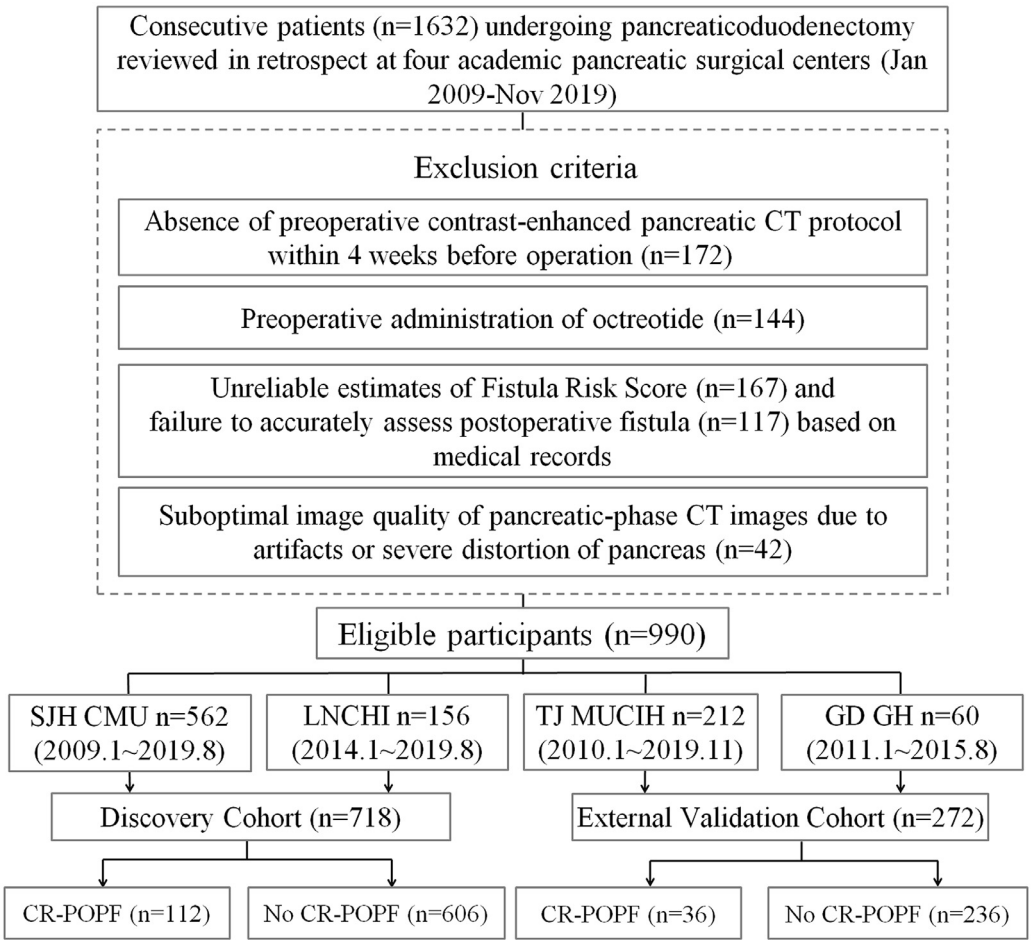

Fig. 1. Schematic of study design. CR-POPF: clinically relevant postoperative pancreatic fistula; SJH CMU: Shengjing Hospital of China Medical University; LNCHI (Liaoning Cancer Hospital and Institute); TJ MUCIH: Tianjin Medical University Cancer Institute and Hospital; GD GH: Guangdong General Hospital.

non-enhanced phase, as stipulated by current National Comprehensive Cancer Network (NCCN) guidelines [22,23]. A nonionic contrast agent containing iodine (300 mg/mL) was injected at 2–2.5 mL/kg body weight. Median values recorded for timed delays from injection of contrast to starting points of pancreatic parenchymal and portal venous phases were 45 s (IQR, 40–50 s) and 70 s (IQR, 65–75 s), respectively. Acquisition parameters of discovery and validation dataset are listed for comparison in Supplementary Materials (Table S1).

Two experienced abdominal radiologists (primary and secondary raters with 15 and 12 years of experience in pancreatic imaging, respectively) independently measured and evaluated all CT descriptors in pancreatic-phase images using an onsite picture archiving and communication system (PACS) and open-source software (3D Slicer v4.10; www.slicer.org) in the discovery cohort. Inter-rater agreement for each descriptor was subsequently examined. In addition, 200 patients were randomly selected for re-evaluation by the primary rater within at least a 1-month interval to determine intra-rater agreement. Both raters were assisted by an attending surgeon to ensure accurate pinpointing of transection lines. Transection margins were largely at the neck of pancreas, along superior mesenteric vessels, with individual modifications as needed.

CT descriptors, including four scores of semantic features and seven measurements are detailed in Fig. 2 and Supplementary Materials (Text1 and Table S2, definitions and scoring of all features by CT), including visceral fat area (VFA) and various pancreatic parameters (thickness, width, stump area, remnant pancreatic volume [RPV], surface area-to-volume [Sa/V] ratio, and mean attenuation). Scored semantic features (Supplementary Materials, Figure S1) were CT-based fatty change (0–3), pancreatic inflammation (0–3), degree of pancreatic atrophy (0–3), and MPD (0–4). Several of the latest reporting standards or global guidelines for diffuse pancreatic diseases [24-26] or FRS appraisal [13,14] of MPD were availed for this purpose.

2.4. Clinical data collection, FRS calculation, and preventive treatments

Five lead pancreatic surgeons averaging ≥20 PDs per year performed all pancreaticoenteric reconstructions after PDs in conjunction with either pancreaticojejunostomy (PJ) or pancreaticogastrostomy (PG) for a full array of indications. Both in discovery and validation datasets, qualifying patients underwent preoperative standardized pancreatic CE-CT imaging studies that documented of all four FRS elements. Medical records were accessed for demographic and clinical parameters, including age, sex, BMI, diabetes mellitus, jaundice, smoking, excessive drinking (average alcohol consumption exceeding 40 g/day in men and 20 g/day in women), and operative factors (Table 1). Clinical data collection and overall clinical outcomes are detailed in Supplementary Materials (Text 2).

Grading of POPFs was dictated by definitions of the International Study Group of Pancreatic Fistula (ISGPF) updated in 2016 [8,12] (see Supplementary Materials, Table S3). The four risk factors required for FRS determinations (see Supplementary Materials, Table S4), operative time and type of anastomosis were obtained from operative notes recorded retrospectively or prospectively during surgery and housed in a prospectively maintained database. Through intraoperative palpation, experienced lead surgeons subjectively characterized pancreatic texture as soft or firm, regardless of histopathology. MPD size (mm) was

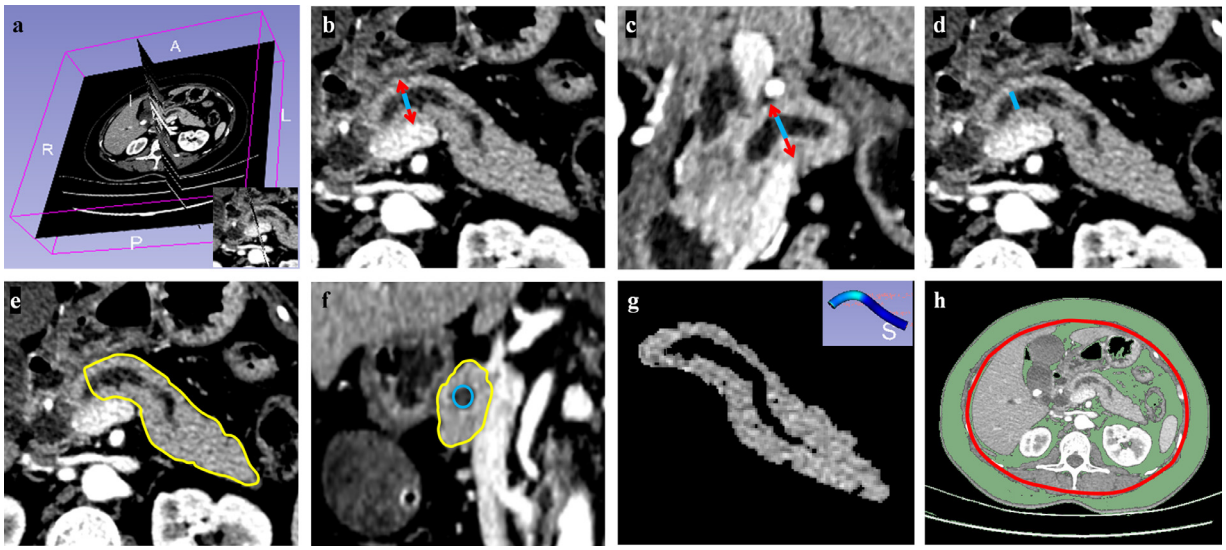

Fig. 2. Representative preoperative CT images of segmentations and morphologic depictions of pancreatic remnant: (a) estimated transection line in 3D-Slicer; (b) transverse section for measuring pancreatic thickness (red arrow), subtracting diameter of main pancreatic duct (MPD, blue line) from parenchymal thickness for final figure and evaluating pancreatic atrophy by MPD-to-parenchymal thickness ratio (MPD / [thickness − MPD]) described in Table S2; (c) coronal section for measuring full pancreatic width (red arrow), subtracting MPD diameter (blue line) for final figure; (d) transverse section for measuring MPD diameter (blue line) for 0–4 scoring of Fistula Risk Score (FRS) as calculated in Table S4; (e) surface area encircled by yellow lines, indicating full pancreatic remnant; (f) Full pancreatic stump area (encircled by yellow lines) calculated by subtracting the visible MPD area from entire area of stump; (g) estimate of pancreatic remnant volume using Otsu's thresholding method (>25 HU) for automated subtraction of MPD volume from full pancreatic remnant volume by segmentation, the mean attenuation represented by mean HU value of all pixels within volume; and (h) assessment of visceral fat area (VFA).

assessed in axial images of the most recent preoperative CT scans or evaluated intraoperatively by placing flexible rulers (if available) against cut surfaces of transected pancreas. FRS values (0–10) were categorized as low (0–2), moderate (3–6), or high (7–10) levels of risk.

The strategies invoked for fistula mitigation reflected surgeon-based preferences. Two intraoperative laminar intraperitoneal drains were routinely placed in nearly all patients (>98%). Postoperative somatostatin analogs (eg, Octreotide) were administered to 517 patients (52.2%), and transanastomotic stents were deployed for internal drainage in 567 patients (57.3%). Use of surgical tissue adhesives was negligible (<1%).

2.5. Histologic evaluation of pancreatic stump

In the prospectively recorded cohort of the discovery dataset, all specimens of pancreatic stump were collected intraoperatively. Samples were routinely processed to evaluate glandular atrophy and lipomatosis in hematoxylin and eosin (HE)-stained slide preparations, using Masson's trichrome and picrosirius red stains to quantify and stage tissue fibrosis. Histologic changes were evaluated by consensus of two dedicated pathologists (each with >10 years of experience in pancreatic pathology) who were blinded to clinical data and radiologic findings. Exocrine glandular atrophy (A0-A2) was graded by the state of viability as normal (A0, 75–100%), mild (A1, 25–75%), or severe (A2, 0–25%) [27]. Degrees of lipomatosis (L0-L3), including both intra- and interlobular fatty content, were graded as normal (L0, 0–10%), mild (L1, 10–20%), marked (L2, 20–30%), or severe (L3, >30%) [28,29]. Stages of pancreatic fibrosis (F0-F3) were assigned as follows: normal pancreatic parenchyma (F0), mild fibrosis with thickening of periductal fibrous tissue (F1), moderate fibrosis with marked sclerosis of interlobular septa and no evidence of architectural changes (F2), or severe fibrosis with detection of architectural destruction (F3) [30].

2.6. Statistical analysis

Descriptive statistics (ie, continuous variables), expressed as median and interquartile range (IQR: 25th-75th percentiles) values, were compared via Wilcoxon rank-sum test. Categorical variables were expressed as counts and percentages, using Chi-Square or Fisher's exact test as warranted for comparisons. To impute missing data, we used means in numeric columns, medians in integer columns, and most frequent values in non-numeric columns.

Model establishment: Intraclass correlation coefficients (ICCs) of each CT predictor reflected inter- and intra-rater agreement levels of the two radiologists. Further consideration of corresponding predictors was precluded at ICC values <0.75 [31]. Candidate risk factors included CT descriptors, demographics, FRS elements, operative parameters, and fistula preventive treatments. Risk factors for CR-POPF demonstrating significance ($p<0.1$) in univariate logistic regression analysis were initially incorporated into multivariable models. Such robust variables were first analyzed by Spearman's correlation to identify paired factors with strong multicollinearity (correlation coefficient $r>0.7$), excluding the less prognostic factors to reduce redundancy. The emerging significant and non-redundant variables subsequently served for model establishment. To devise a robust multivariate logistic regression model without overfitting, two multivariate models were compared: one full model defining all qualified risk factors through backward elimination, and the other a simplified version invoking the least absolute shrinkage and selection operator (LASSO) method to select useful variables [32]. Penalty parameters of LASSO were determined by 10-fold cross validation via minimum mean cross-validated error, achieving a parsimonious model with fewer included variables but minor loss of predictive ability [33].

Model performance: By design, we explored the potential for CT to augment the FRS in predicting CR-POPF at various levels of risk. Performance levels of both CT-FRS (full or simplified) and FRS models were individually plotted, expressed as areas under receiver operating characteristic curves (AUC or C-statistic values), and compared by Delong test [34]. McNemar's test was then applied to compare measures of diagnostic accuracy.

Presumptive correlations between CT-FRS probabilities (or single CT predictors) and histologic findings were later addressed using Spearman's correlation coefficient. Model establishment and model performance were tested in the R environment (v3.5.0; R Project for Statistical Computing, Vienna, Austria), comparing related variables (eg, AUC, accuracy) using MedCalc (v15.6.1; MedCalc Software, Ostend, Belgium). Other descriptive statistics were reliant on SPSS

Table 1
Demographic and clinicopathologic characteristics of patients.

Characteristic	Discovery cohort (n = 718)	Validation cohort (n = 272)	P
Patient characteristics			
Age, yrs	59 (53–66)	60 (53–65)	0.376
BMI, kg/m^2	23 (20.9–24.9)	23 (21.3–25.2)	0.088
Sex, male	300 (41.8)	128 (47.1)	0.154
Diabetes mellitus, yes	172 (24.0)	83 (30.5)	**0.043**
Jaundice, yes	351 (48.9)	124 (45.6)	0.392
Smoking, yes	333 (46.4)	127 (46.7)	0.987
Excessive drinking	264 (36.8)	103 (37.9)	0.806
ASA-PS, 0/1/2/3	108/481/115/14	35/172/54/11	0.103
CT predictors			
Thickness, mm	22.8 (19.1–26.4)	21.9 (17.4–27.4)	0.526
Width, mm	20.5 (16.6–24.8)	21.3 (16.6–25.9)	0.122
Stump area, cm^2	3.5 (2.2–4.9)	3.4 (1.9–5.1)	0.728
MPD, mm	4.0 (2.1–6.2)	4.2 (2.2–6.2)	0.909
RPV, cm^3	22.3 (12.7–36.1)	22.9 (11.9–34.6)	0.749
Surface, cm^2	6.3 (4.0- 9.0)	6.1 (3.6–8.5)	0.334
Sa/V ratio	0.289 (0.247–0.308)	0.274 (0.242–0.311)	0.196
Attenuation, HU	72 (57–91)	70 (56–92)	0.222
VFA, cm^2	84 (55–111)	81 (47–94)	0.322
Inflammation, 0/1/2/3	442/178/96/2	140/80/50/2	**0.024**
Fatty change, 0/1/2/3	192/336/186/4	69/144/56/3	0.188
Atrophy, 0/1/2/3	200/260/220/38	100/98/60/14	**0.012**
Operative factors			
Reconstruction, PJ	590 (82.2)	210 (77.2)	0.076
Anastomosis, duct-to-mucosa	495 (83.9)	169 (80.4)	0.257
Operative time, min	488 (448–526)	494 (462–534)	**0.030**
Transanastomotic stent, yes	324 (45.1)	143 (52.6)	**0.042**
Octreotide, yes	369 (51.4)	148 (54.4)	0.437
FRS or a-FRS evaluations			
FRS	3 (1–5)	3 (1–5)	0.260
Gland texture, soft	280 (39)	113 (41.5)	0.510
MPD, mm, ≥5/4/3/2/≤1	306/96/106/156/54	105/46/38/68/15	0.325
Etiology, PDAC or CP	419 (58.4)	148 (54.4)	0.295
Blood loss, ml ≤400, 401–700, 701–1000, >1000	471/213/30/4	190/71/7/4	0.187
CR-POPF, yes	112 (15.6)	36 (13.2)	0.406

Data expressed as n (%) or median (IQR), unless otherwise stated.
Abbreviations:IQR, interquartile range; BMI, body mass index; American Society of Anesthesiologists Physical Status, ASA-PS; MPD, main pancreatic duct; RPV, remnant pancreatic volume; Sa/V ratio, surface area-to-volume ratio; reconstruction, pancreaticojejunostomy (PJ) vs pancreaticogastrostomy (PG); anastomosis, duct-to-mucosa vs end-to-side; FRS, Fistula Risk Score; a-FRS, alternative FRS; VFA, visceral fat area; PDAC, pancreatic ductal adenocarcinoma; CP, chronic pancreatitis; CR-POPF, clinically relevant postoperative pancreatic fistula.
Bold values denote statistical significance at the $p < 0.05$ level.

(v25; IBM Corp, Armonk, NY, USA) for such analyses, setting significance at $p<0.05$. An *a priori* power analysis of sample size via PASS (v11; NCSS, Kaysville, UT, USA) is detailed in the Supplementary Materials (Text 3).

2.7. Role of funding source

Our funding sources had no roles in study design, data handling (collection, analytics, and interpretation), or drafting of the report.

3. Results

3.1. Patient characteristics

Baseline demographics and clinical data, intraoperative data, CT descriptors, and FRS parameters of discovery and validation datasets are presented in Table 1 for purposes of comparison. CR-POPF developed in 15.6% (112/718) of patients within the discovery dataset and in 13.2% (36/272) of patients within the validation dataset, each cohort displaying a median FRS of 3 (IQR: 2–5). With exception of diabetes mellitus, inflammation and atrophy scores, operative time, and stenting implementation, the variables analyzed showed no statistical differences.

3.2. Logistic regression analysis for predicting CR-POPF

Inter- and intra-rater reproducibility of single CT predictors are shown in Supplementary Materials (Table S5), and C-statistics of each predictor for predicting CR-POPF are shown in Supplementary Materials (Table S6 and Figure S2). Significant risk factors for CR-POPF identified by univariate analysis (Table 2) were as follows: higher BMI; non-smoking status; higher-scored FRS elements; and single CT descriptors, including larger pancreatic parameters (VFA, RPV, stump area, thickness, width), lower atrophy and inflammation scores, and higher fat score (except for attenuation).

In multivariate analysis, the simplified logistic regression model of CT-FRS (sCT-FRS) addressed heightened values of the following five risk factors (Fig. 3): RPV (OR per cm^3 increase=1.041, 95%CI: 1.024–1.058), stump area (OR per cm^2 increase=1.159, 95%CI: 1.027–1.309), fat score (OR per point=1.458, 95%CI: 1.059–2.007), atrophy score (OR per point=0.601, 95%CI: 0.428–0.845), and scored MPD (OR per point=1.591, 95%CI: 1.303–1.944). Probability of CR-POPF was calculated as follows:

$$Odds = exp(-4.294 + 0.040[RPV] + 0.15[Area] - 0.465[Duct] + 0.377[Fat] - 0.508[Atrophy]);$$

$$Probability = odds/(1 + odds);$$

The equations for full CT-FRS model and a-FRS model were detailed in Supplementary Materials (Text 4).

The Online calculator website for the estimated probability using simplified CT-FRS model is https://app.calculoid.com/#/calculator/75123. The examples were detailed in Text 4.

3.3. Performance of all models for prediction of CR-POPF

Performance levels of the full and simplified CT-FRS models, FRS and a-FRS are provided (Table 3) for comparison**.** Since both full and simplified CT-FRS models performed similarly in predicting CR-POPF occurrences of discovery (AUC: 0.828 vs 0.825; p = 0.764 [Delong test]) and validation (AUC: 0.804 vs 0.807; p = 0.787 [Delong test]) datasets, the results from the simplified model were employed for further analysis. The sCT-FRS significantly outperformed the FRS (discovery: AUC=0.794; p = 0.04 [Delong test]; validation: AUC=0.741; and p = 0.05 [Delong test]) and the a-FRS (discovery: AUC=0.792; p = 0.03 [Delong test]; validation: AUC=0.716; p = 0.005 [Delong test]).

When stratified by FRS, there were 340 (47.4%) and 146 (53.7%) patients of moderate risk level in discovery and validation datasets, respectively. However, the simplified model yielded a remarkably higher AUC value, relative to the original FRS (discovery: 0.729 vs 0.626 [p = 0.002, Delong test]; validation: 0.722 vs 0.573 [p = 0.017, Delong test]) and a-FRS (discovery: 0.649 [p = 0.012, Delong test]; validation: 0.530 [$p<0.001$, Delong test]), for this moderate-risk subset (Table 3 and Fig. 4). In patients at low and high risk levels by FRS, the sCT-FRS did not differ significantly with either FRS or a-FRS, whether applied to discovery or validation subjects (Supplemental Table S7).

3.4. Histopathologic correlations

As shown in Fig. 5, the probabilities generated by simplified model were significantly higher for patients with CR-POPF than for those without CR-POPF within all stages/grades of pancreatic fibrosis, glandular atrophy, and lipomatosis. They strongly and negatively

Table 2
Univariate and multivariate logistic regression analyses of risk factors for clinically relevant postoperative pancreatic fistula (CR-POPF).

	Univariate analysis		Multivariate analysis, OR (95% CI)			
	OR (95% CI)	*P*	Full model	*P*	Simplified model	*P*
Demographics						
Age, >60 yrs	0.790 (0.525–1.189)	0.259	–		–	
BMI, per kg/m^2	1.187 (0.988–1.426)	**0.068**	1.029 (0.943–1.123)	0.521	†	
Sex, male	1.148 (0.765–1.724)	0.504	–		–	
Diabetes, yes	0.844 (0.518–1.375)	0.496	–		–	
Jaundice, yes	1.303 (0.870–1.953)	0.199	–		–	
Smoking status, yes	1.669 (1.112–2.513)	**0.014**	†		†	
Excessive drinking, yes	1.240 (0.822–1.872)	0.305	–		–	
ASA-PS						
1	–	–				
2	1.316 (0.652–2.657)	0.443	–		–	
3/4	1.139 (0.654–1.986)	0.646	–		–	
Operation						
Operative time, per IQR	1.095 (0.917–1.308)	0.315	–		–	
Reconstruction, PJ	1.267 (0.727–2.208)	0.404	–		–	
Octreotide, yes	1.374 (0.914–2.065)	0.127	–		–	
Anastomosis, duct-to-mucosa	0.856 (0.558–1.312)	0.475	–		–	
Stent, yes	1.465 (0.914–2.347)	0.112	–		–	
Surgeon	1.122 (0.840–1.498)	0.435	–		–	
CT measurements						
Attenuation, per HU	1.003 (0.996–1.009)	0.397	–		–	
Thickness, per mm	1.089 (1.053–1.125)	<**0.001**	*		*	
Width, per mm	1.049 (1.019–1.080)	**0.001**	*		*	
Sa/V ratio, per 0.1	0.003 (0.001–0.085)	**0.001**	†		†	
Stump area, per cm^2	1.303 (1.190–1.428)	**0.010**	1.228 (1.072–1.406)	**0.003**	1.159 (1.027–1.309)	**0.017**
RPV, per cm^3	1.065 (1.050–1.081)	<**0.001**	1.040 (1.023–1.058)	<**0.001**	1.041 (1.024–1.058)	<**0.001**
VFA, per cm^2	1.009 (1.004–1.015)	**0.002**	†		†	
CT evaluation, per point						
Inflammation	0.522 (0.368–0.740)	<**0.001**	0.712 (0.469–1.082)	0.111	†	
Fat	1.354 (1.030–1.781)	**0.030**	1.519 (1.094–2.109)	**0.013**	1.458 (1.059–2.007)	**0.021**
Atrophy	0.313 (0.232–0.422)	<**0.001**	0.654 (0.458–0.933)	**0.019**	0.601 (0.428–0.845)	**0.003**
FRS items						
Gland texture	2.040 (1.644–2.530)	<**0.001**	†		†	
MPD	2.358 (1.932–2.877)	<**0.001**	1.568 (1.28–1.922)	<**0.001**	1.591 (1.303–1.944)	<**0.001**
Etiology	1.928 (1.034–3.594)	**0.039**	1.576 (0.938–2.65)	0.086	†	
Blood loss	1.593 (1.173–2.164)	**0.003**	†		†	

Factors in multivariable analysis showed significance ($p<0.1$, bolded) by univariate analysis.
* Significant parameters excluded from multivariate logistic model due to strong collinearity (Spearman's correlation coefficient >0.7).
† Significant parameters excluded from multivariate logistic model through backward elimination in full model or LASSO selection in simplified model
Abbreviations: OR, odds ratio; BMI, body mass index; Sa/V ratio, surface area-to-volume ratio; CI, confidence interval; Drain placement, two vs three intraoperative laminar intraperitoneal drains; American Society of Anesthesiologists Physical Status, ASA-PS; reconstruction, pancreaticojejunostomy (PJ) vs pancreaticogastrostomy (PG); Anastomosis of PJ, duct-to-mucosa vs end-to-side; RPV, remnant pancreatic volume; VFA, visceral fat area; FRS, Fistula Risk Score; MPD, main pancreatic duct.

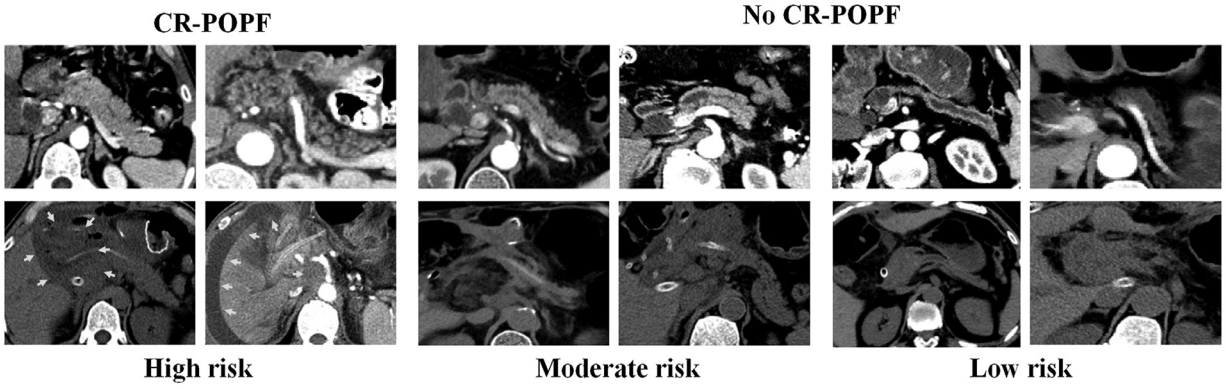

Fig. 3. Preoperative (first row) and postoperative (second row) CT images of patients with differing CT-FRS probabilities of developing clinically relevant postoperative pancreatic fistula (CR-POPF): (1) high-risk patients in columns 1–2 (probabilities: 0.709 and 0.485, respectively) with large remnant pancreatic volumes, small-sized main pancreatic ducts (MPDs size <2 mm), non-atrophic parenchyma (atrophy score ≤ 1), substantial stump areas, and fatty pancreatic remnants that increase CR-POPF risk, all showing intra-abdominal and perianastomotic fluid collection (green arrows) on postoperative CT images; (2) moderate-risk patients in columns 3 and 4 (probabilities: 0.195 and 0.134, respectively) with moderate-sized MPDs (2–5 mm) and slightly atrophic volumes, one (column 3) developing biochemical POPF and the other (column 4) devoid of CR-POPF, any type; and (3) low-risk patients in columns 5 and 6 with small atrophic glands and large-sized MPDs (>5 mm) (probabilities: 0.061 and 0.037, respectively) showing the least risk of CR-POPF, neither developing any type of CR-POPF.

Table 3
Predictive performances of various models in all-risk and moderate-risk (FRS: 3–6) groups of Discovery and validation cohorts.

All risk	C-statistic (95% CI)	Accuracy (95% CI)	Sensitivity (95% CI)	Specificity (95% CI)
CT-FRS (Full model)				
Discovery	0.828 (0.784–0.872)	79.0 (76.9–81.0)	76.8 (69.0–84.6)	79.4 (76.2–82.6)
Validation	0.804 (0.732–0.877)	68.0 (64.9–71.2)	86.1 (74.8–97.4)	65.3 (59.2–71.3)
CT-FRS (Simplified model)				
Discovery	0.825 (0.782–0.868)	78.3 (75.1–81.2)	75.9 (67.9–83.9)	78.7 (75.4–81.9)
Validation	0.807 (0.739–0.875)	62.9 (59.7–66.0)	91.7 (82.6–100.0)	58.5 (52.2–64.8)
FRS				
Discovery	0.794 (0.752–0.835)	71.2 (68.1–74.2)	76.8 (69.0–84.6)	70.1 (66.5–73.8)
Validation	0.741 (0.663–0.819)	53.3 (50.1–56.5)	91.7 (82.6–100.0)	47.5 (41.1–53.8)
a-FRS				
Discovery	0.792 (0.760–0.821)	74.6 (70.9–78.0)	73.2 (64.0–81.1)	74.9 (71.3–78.3)
Validation	0.716 (0.658–0.768)	57.7 (52.1–63.3)	86.1 (70.5–95.3)	53.4 (46.8–59.9)
Moderate risk	C-statistic (95% CI)	Accuracy (95% CI)	Sensitivity (95% CI)	Specificity (95% CI)
CT-FRS (Full model)				
Discovery	0.746 (0.696–0.791)	67.9 (65.8–70.1)	80.5 (70.3–88.4)	64.0 (57.8–69.8)
Validation	0.719 (0.618–0.819)	73.3 (71.0–75.6)	65.5 (45.7–82.1)	75.2 (66.4–82.7)
CT-FRS (Simplified model)				
Discovery	0.729 (0.678–0.775)	65.6 (63.5–67.7)	78.0 (67.5–86.4)	61.6 (55.4–67.6)
Validation	0.722 (0.626–0.819)	73.3 (71.0–75.6)	62.1 (42.3–79.3)	76.1 (67.3–83.5)
FRS				
Discovery	0.626 (0.573–0.678)	58.2 (57.1–59.4)	69.5 (58.4–79.2)	54.7 (48.4–60.8)
Validation	0.573 (0.455–0.69)	69.9 (68.6–71.1)	37.9 (20.7–57.7)	77.8 (69.2–84.9)
a-FRS				
Discovery	0.649 (0.596–0.700)	52.9 (46.4–58.8)	80.5 (70.3–88.4)	44.2 (38.0 - 50.5)
Validation	0.530 (0.445–0.613)	41.1 (35.0–47.4)	82.8 (64.2–94.2)	30.8 (22.6 - 40.0)

Data expressed as fraction or% (95% CI).
Abbreviations: CT-FRS, CT-adjusted Fistula Risk Score (FRS); CI, confidence interval; a-FRS, alternative FRS.

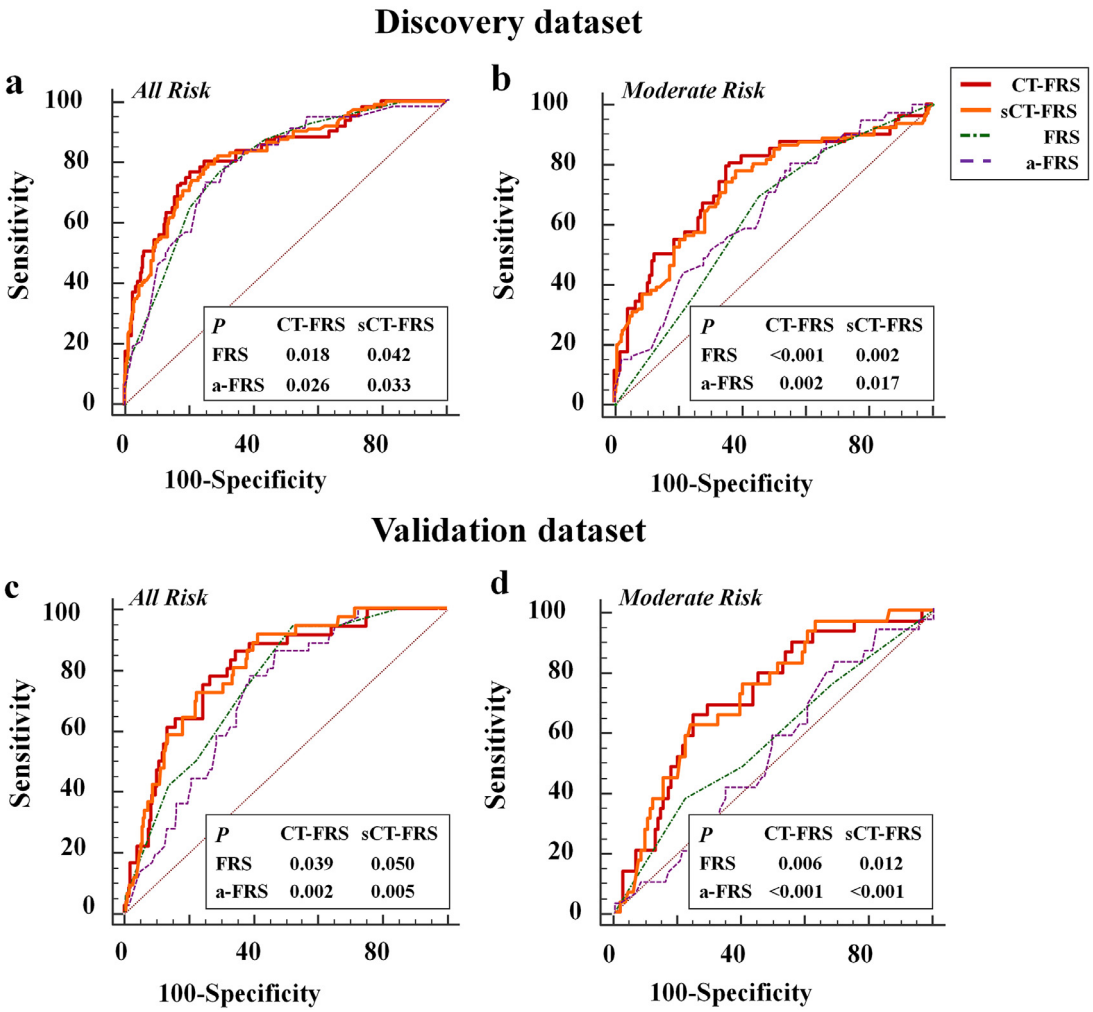

Fig. 4. Predictive performances of FRS, a-FRS, the full CT-FRS model and the simplified CT-FRS (sCT-FRS) model in predicting CR-POPF: Receiver operating characteristic (ROC) curves of FRS, a-FRS, CT-FRS, and sCT-FRS predictive models are plotted for (a, b) discovery and (c, d) validation cohorts. In all patients and in those with moderate risk by FRS, the two CT-FRS models fared significantly better than the original FRS and a-FRS, whereas the full and simplified CT-FRS models did not differ significantly at each task.

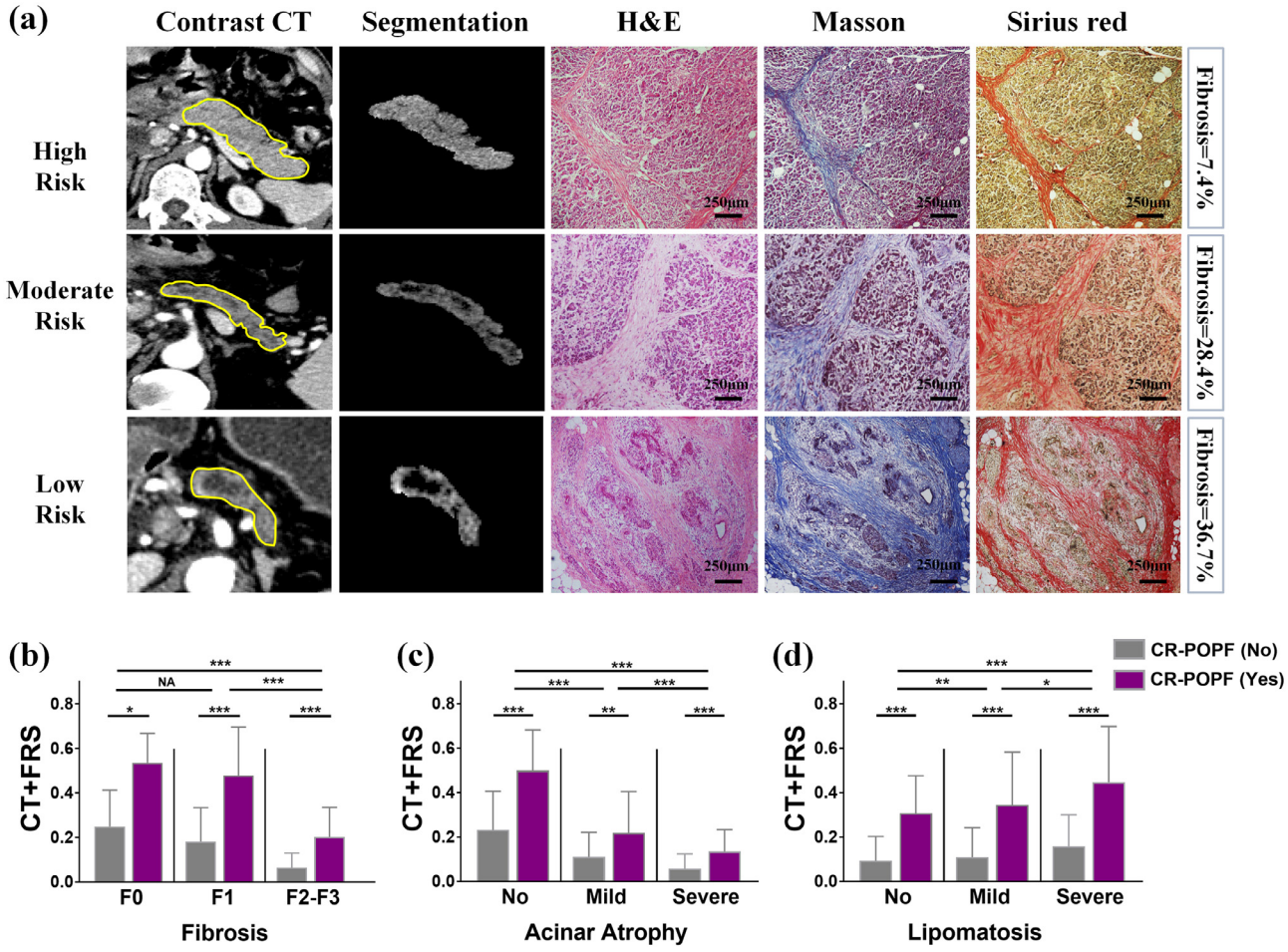

Fig. 5. Preoperative CT findings and postoperative histologic evaluations of pancreatic stumps: (a) preoperative CT scans of patients with differing CR-POPF risks are shown, ranging from high (first row) to moderate (second row) and low (third row) risk based on CT-FRS model. In the first column, ROIs are delineated in pancreatic remnants, whereas the segmented pancreatic remnants of second column exclude ductal volumes. The final three columns reveal histologic features of remnant pancreas stained by H&E, Masson's trichrome, and Sirius Red, respectively. From high to low risk, both pancreatic fibrosis and glandular atrophy had progressed; and (b-d) CT-FRS probabilities correspond with stages of fibrosis (F0, F1, F2-F3), degrees of glandular atrophy (no [A0], mild [A1] and severe [A2]), and extents of lipomatosis (no [L0], mild [L1-L2], severe [L3]), decreasing as fibrosis and glandular atrophy advance, and increasing as lipomatosis advances. All CT-FRS probabilities in CR-POPF risk groups (purple columns) were significantly higher than those in non CR-POPF groups (gray columns) at each histologic stage or grade. Scale bars represent 250 μm.

correlated with increasing stages of fibrosis (r=−0.568; p<0.001) or degrees of glandular atrophy (r = −0.529; p<0.001), but positively correlated with advancing lipomatosis (r = 0.137; p<0.001).

Individually, the correlations between pancreatic stump histology and preoperative CT findings are detailed in Supplemental Table S8. The CT-based scores of atrophy (r = 0.727; p<0.001) and fat (r = 0.540, p<0.001) strongly correlated with histologic grades of glandular atrophy and lipomatosis, respectively. VFA also positively correlated with lipomatosis (r = 0.416; p<0.001). A softened pancreas positively correlated with CT fat score (r = 0.410; p<0.001), CT atrophy score (r = −0.449; p<0.001) and negatively correlated with MPD score (r = −0.485; p<0.001).

4. Discussion

In the course of this study, we developed and externally validated the CT-FRS model as a modification of the established FRS. By adding pancreatic CE-CT to the FRS framework, overall predictive performance levels (C-indices) of 0.80−0.83 were achieved in discovery and external testing cohorts. The CT-FRS model substantially improved FRS predictive capability, specifically in patients at moderate levels of risk (FRS: 3−6). Discounting earlier FRS elements of etiology, blood loss, and gland texture, it relies instead on MPD size, RPV, stump area, and CT-scored fatty change and atrophy as critical features. Ultimately, CT-FRS probabilities showed significant associations with histologically advanced lipomatosis, ample glandular acini, and less pancreatic fibrosis.

As opposed to sophisticated quantitative imaging methods mired in complex and confusing technology, we turned to simple, efficient, and universal predictors that clinicians may readily ascertain via hospital information systems (eg, PACS) or through open-source software (eg, 3D-slicer, ITK-Snap). In theory, POPFs are likely to originate from soft and large anastomotic stumps [8], so non-atrophic, large RPVs with higher fat scores, larger stump areas, and small-sized MPDs (reflecting full tissue viability) present the greatest threat of CR-POPF in our CT-FRS model. A sizeable, non-atrophic RPV is capable of secreting more activated pancreatic fluid, and large stump areas require more extensive suturing, increasing the likelihood of anastomotic failure. Moreover, a fatty and non-atrophic pancreas, imparting softer gland texture (correlating strongly in our study), and a small-caliber MPD are clearly problematic in terms of anastomotic integrity.

There is mounting published evidence that quantitative CT images may offer a non-invasive approach to predicting CR-POPF [18-20,35,36]. Yujiro and Mitsureo have indicated that CT-based RPV and visceral adipose tissue measurements from CT images could be promising in this regard (AUC >0.85), although both sources analyzed single-center data, without external validation or direct comparison

with FRS [19,20,35]. By contrast, our CT-FRS models incorporated nearly all published CT-based descriptors [18-20,35-39] for rigorous training and external validation. The final simplified model was confined to five factors, without any C-statistical sacrifice relative to the full model. Moreover, it surpassed the FRS model and any other single CT predictor, demonstrating statistical superiority. Roberts et al. have also used three CT-based perioperative descriptors to predict POPF, examining 107 patients treated at a single institution [40]. They found pancreatic duct width to be the sole independent variable related to POPF, similar to our observations. Unlike our analysis, however, steatosis and POPF showed no relation. Furthermore, they did not assess the performance of their predictive model (ie, no AUC or accuracy measures), so we were unable to directly compare our model with theirs in terms of performance. One recent study has claimed that CT radiomics produced AUC values 0.82 and 0.76 in 80 training and in 37 test subjects, respectively [41]. Our CT-FRS has shown similar predictive capability, albeit with much stronger statistical power given the large sample size.

When first reported, the FRS was credited with a very high AUC (>0.9). Unfortunately, such values declined (0.7−0.8) in external validation datasets of ensuing publications [14,15]. This was perhaps due to overfitting in the original discovery dataset or subjectivity of some FRS elements (eg, pancreatic texture) that weakened its applicability. In our study, a soft-to-touch pancreas was significant by univariate analysis but excluded during final multivariate analysis. We therefore presumed that this facet is best represented by other significant CT predictors (eg, large RPV, stump area, and higher CT-based fat score and lower atrophy score), which correlate with histologic less fibrosis and greater lipomatosis [30,39]. The newer a-FRS substitutes BMI for blood loss and etiology used in the original FRS [16]. Higher BMI implies a fatty/soft pancreas [16,29,42] and is a widely reported determinant of CR-POPF risk. Herein, both the CT-based fat score and BMI proved significant in our univariate analysis, although the fat score was more prognostically sound and directly signified pancreatic fat infiltration. It was thus included in our final CT-FRS model. Factors other than high BMI, such as old age and diabetes or other metabolic syndromes [26], have also been known to increase pancreatic fat. Hence, it is likely that local fatty change at pancreas, rather than high BMI, is the fundamental risk factor or CR-POPF. We also found that CT-FRS enhancement of the FRS is conferred at moderate risk levels only (FRS: 3−6). For low-risk (FRS: 0−2) or high-risk (FRS: 7−10) subjects, in whom CR-POPF are either unlikely or very much inclined to happen, the diagnostic accuracies of FRS and CT-FRS were similarly quite good. The CT-FRS is thus advantageous in patients with moderate risk by FRS.

Our CT-FRS model directly computes the probability that CR-POPF will develop. Using the equation provided herein or available in the online calculator (https://app.calculoid.com/#/calculator/75123), input of five items yields an instant numerical determination. Results of a recently conducted global survey indicate that surgeons vary greatly in their management to prevent and minimize POPF [43], so there is likely room for improvement. The CT-FRS stands to help surgeons objectify POPF risk in their design, study, and implementation of decision trees, perhaps when selecting patients for somatostatin analogues or for placement of surgical drains. In low-risk patients, a no-drain strategy would apply. This is especially relevant, as outcomes of several current studies have underscored the complications imposed by these surgical drains [44,45]; and because reductions in absolute risk do not justify the expense, costly somatostatin analogues may be eliminated [46]. In high-risk patients (probability>0.15), use of somatostatin analogues would then rely on objective evidence rather than discretionary preferences. Finally, CT-FRS scoring may have a role in evaluating surgical technical performance or treatment stratification.We do acknowledge some limitations of this study. First, this was a retrospective investigation involving both prospectively and retrospectively maintained databases. Prospective studies conducted at high-volume centres are essential going forward to further validate our results; and interventional randomized controlled trials (RCTs) might well be pursued, using CT-FRS probabilities for therapeutic guidance. Another issue is that the CT-FRS requires manual evaluations by radiologists. Eventually, automated methods such as deep-network artificial intelligence may become available and offer more convenience. Although CE-CT is stipulated by NCCN guidelines in patients with pancreatic cancer [22], this constraint may narrow the scope of CT-FRS. Finally, there was no significant benefit attached to reconstruction technique, octreotide analog treatment, or transanastomotic stenting in terms of reducing CR-POPOF in these patients. However, mixed results of RCTs and meta-analyses have been shown in the past year [47−49], calling for more focused assessments of preventive strategies.

In conclusion, we developed and externally validated a CT-FRS model for predicting CR-POPF in patients with pancreaticoenteric anastomoses after PD. By addressing five critical elements (pancreatic volume, stump area, MPD size, and CT-based scoring of atrophy and fat), the CT-FRS model improved the predictive performance of FRS particularly in moderate-risk patients. The probabilities of CR-POPF generated by CT-FRS reflect less tissue fibrosis, more lipomatosis, and an abundance of glandular acini at pancreatic stump. Future research should focus on prospective RCT studies, incorporating the CT-FRS into surgical planning for optimal decision-making and patient care.

Contributors

Guarantor of the article: Yu Shi

Conception and design: Yu Shi, Feng Gao

Acquisition of data: Yu Shi, Feng Gao, Youli Xu, Xianyi Zhang, Xiaoli Cai

Analysis and interpretation of data: Yu Shi, Youli Xu, Xianyi Zhang, Xiaoli Cai

Drafting of manuscript: Yu Shi, Feng Gao, Yafei Qi, Hong Lu

Critical revision: Yu Shi, Feng Gao, Yafei Qi, Hong Lu, Fulu Ai, Yang Hou, Chang Liu, Youli Xu, Xianyi Zhang, Xiaoli Cai

Yu Shi and Feng Gao contributed equally to this manuscript as the co-first authors.

All the authors read and approved the final version of the manuscript.

Funding sources

This paper was supported by the National Natural Science Foundation of China (82071885, 81771802, 81771893, 81901741) and the Support Program for Innovative Talents in Universities of Liaoning Province (Grant No. LR2016020).

Data sharing

http://dx.doi.org/10.17632/5jspp7fj82.2

Declaration of Competing Interest

None of the authors has any conflict of interest to declare. Yu Shi and Feng Gao contributed equally to this manuscript as the co-first authors.

Supplementary materials

Supplementary material associated with this article can be found, in the online version, at doi:10.1016/j.ebiom.2020.103096.

References

[1] Nakeeb A, Lillemoe KD, Cameron JL. The role of pancreaticoduodenectomy for locally recurrent or metastatic carcinoma to the periampullary region. J Am Coll Surg 1995;180(2):188–92.
[2] Büchler MW, Wagner M, Schmied BM, Uhl W, Friess H, Z'graggen K. Changes in morbidity after pancreatic resection: toward the end of completion pancreatectomy. Arch Surg 2003;138(12):1310–4.
[3] Poon RTP, Lo SH, Fong D, Fan ST, Wong J. Prevention of pancreatic anastomotic leakage after pancreaticoduodenectomy. Am J Surg 2002;183(1):42–52.
[4] Nahm CB, Connor SJ, Samra JS, Mittal A. Postoperative pancreatic fistula: a review of traditional and emerging concepts. Clin Exp Gastroenterol 2018;11:105–18.
[5] Pedrazzoli S. Pancreatoduodenectomy (PD) and postoperative pancreatic fistula (POPF): a systematic review and analysis of the POPF-related mortality rate in 60,739 patients retrieved from the English literature published between 1990 and 2015. Medicine (Baltimore) 2017;96(19):e6858.
[6] Qiu J, Du C. Pancreatogastrostomy Versus Pancreatojejunostomy for RECOnstruction After PANCreatoduodenectomy (RECOPANC, DRKS 00000767): perioperative and long-term results of a multicenter randomized controlled trial. Ann Surg 2017;266(6):e63–e4.
[7] Fu SJ, Shen SL, Li SQ, et al. Risk factors and outcomes of postoperative pancreatic fistula after pancreatico-duodenectomy: an audit of 532 consecutive cases. BMC Surg 2015;15:34.
[8] Bassi C, Marchegiani G, Dervenis C, et al. The 2016 update of the International Study Group (ISGPS) definition and grading of postoperative pancreatic fistula: 11 Years After. Surgery 2017;161(3):584–91.
[9] Shrikhande SV, Sivasanker M, Vollmer CM, et al. Pancreatic anastomosis after pancreatoduodenectomy: a position statement by the international study group of pancreatic surgery (ISGPS). Surgery 2017;161(5):1221–34.
[10] Pedrazzoli S, Liessi G, Pasquali C, Ragazzi R, Berselli M, Sperti C. Postoperative pancreatic fistulas: preventing severe complications and reducing reoperation and mortality rate. Ann Surg 2009;249(1):97–104.
[11] Kawaida H, Kono H, Hosomura N, et al. Surgical techniques and postoperative management to prevent postoperative pancreatic fistula after pancreatic surgery. World J Gastroenterol 2019;25(28):3722–37.
[12] Bassi C, Dervenis C, Butturini G, et al. Postoperative pancreatic fistula: an international study group (ISGPF) definition. Surgery 2005;138(1):8–13.
[13] McMillan MT, Soi S, Asbun HJ, et al. Risk-adjusted outcomes of clinically relevant pancreatic fistula following pancreatoduodenectomy: a model for performance evaluation. Ann Surg 2016;264(2):344–52.
[14] Miller BC, Christein JD, Behrman SW, et al. A multi-institutional external validation of the fistula risk score for pancreatoduodenectomy. J Gastrointest Surg 2014;18(1):172–9 discussion 9-80.
[15] Callery MP, Pratt WB, Kent TS, Chaikof EL, Vollmer Jr. CM. A prospectively validated clinical risk score accurately predicts pancreatic fistula after pancreatoduodenectomy. J Am Coll Surg 2013;216(1):1–14.
[16] Mungroop TH, van Rijssen LB, van Klaveren D, et al. Alternative Fistula risk score for pancreatoduodenectomy (a-FRS): design and international external validation. Ann Surg 2019;269(5):937–43.
[17] Grendar J, Jutric Z, Leal JN, et al. Validation of Fistula risk score calculator in diverse North American HPB practices. HPB (Oxford) 2017;19(6):508–14.
[18] Okano K, Oshima M, Kakinoki K, et al. Pancreatic thickness as a predictive factor for postoperative pancreatic fistula after distal pancreatectomy using an endopath stapler. Surg Today 2013;43(2):141–7.
[19] Frozanpor F, Loizou L, Ansorge C, Segersvärd R, Lundell L, Albiin N. Preoperative pancreas CT/MRI characteristics predict Fistula rate after pancreaticoduodenectomy. World J Surg 2012;36(8):1858–65.
[20] Kirihara Y, Takahashi N, Hashimoto Y, et al. Prediction of pancreatic anastomotic failure after pancreatoduodenectomy: the use of preoperative, quantitative computed tomography to measure remnant pancreatic volume and body composition. Ann Surg 2013;257(3):512–9.
[21] Collins GS, Reitsma JB, Altman DG, Moons KG. Transparent Reporting of a multivariable prediction model for individual prognosis or diagnosis (TRIPOD): the TRIPOD statement. Br J Surg 2015;102(3):148–58.
[22] Tempero MA, Malafa MP, Al-Hawary M, et al. Pancreatic adenocarcinoma, version 2.2017, NCCN clinical practice guidelines in oncology. J Natl Compr Canc Netw 2017;15(8):1028–61.
[23] Tempero MA, Malafa MP, Chiorean EG, et al. Pancreatic adenocarcinoma, version 1.2019. J Natl Compr Canc Netw 2019;17(3):202–10.
[24] Tirkes T, Shah ZK, Takahashi N, et al. Reporting standards for chronic pancreatitis by using CT, MRI, and MR cholangiopancreatography: the consortium for the study of chronic pancreatitis, diabetes, and pancreatic cancer. Radiology 2019;290(1):207–15.
[25] Harshit Kumar A, Singh Griwan M. A comparison of APACHE II, BISAP, Ranson's score and modified CTSI in predicting the severity of acute pancreatitis based on the 2012 revised Atlanta classification. Gastroenterol Rep (Oxf) 2018;6(2):127–31.
[26] Coulier B. Pancreatic lipomatosis: an extensive pictorial review. J Belg Soc Radiol 2016;100(1):39.
[27] Hatano M, Watanabe J, Kushihata F, et al. Quantification of pancreatic stiffness on intraoperative ultrasound elastography and evaluation of its relationship with postoperative pancreatic fistula. Int Surg 2015;100(3):497–502.
[28] Watanabe H, Kanematsu M, Tanaka K, et al. Fibrosis and postoperative Fistula of the pancreas: correlation with MR imaging findings—preliminary results. Radiology 2013;270(3):791–9.
[29] Gaujoux S, Cortes A, Couvelard A, et al. Fatty pancreas and increased body mass index are risk factors of pancreatic fistula after pancreaticoduodenectomy. Surgery 2010;148(1):15–23.
[30] Shi Y, Liu Y, Gao F, et al. Pancreatic stiffness quantified with MR elastography: relationship to postoperative pancreatic Fistula after pancreaticoenteric anastomosis. Radiology 2018;288(2):476–84.
[31] Koo TK, Li MY. A guideline of selecting and reporting intraclass correlation coefficients for reliability research. J Chiropr Med 2016;15(2):155–63.
[32] Marami Milani MR, Hense A, Rahmani E, Ploeger A. Applying least absolute shrinkage selection operator and akaike information criterion analysis to find the best multiple linear regression models between climate indices and components of cow's milk. Foods 2016;5(3).
[33] Vasquez MM, Hu C, Roe DJ, Chen Z, Halonen M, Guerra S. Least absolute shrinkage and selection operator type methods for the identification of serum biomarkers of overweight and obesity: simulation and application. BMC Med Res Methodol 2016;16(1):154.
[34] DeLong E, DeLong D, Clarke-Pearson D. Comparing the areas under two or more correlated receiver operating characteristic curves: a nonparametric approach. Biometrics 1988;44:837–45 *J Clin Pathol: first published as* 2017; 10.
[35] Kanda M, Fujii T, Suenaga M, et al. Estimated pancreatic parenchymal remnant volume accurately predicts clinically relevant pancreatic fistula after pancreatoduodenectomy. Surgery 2014;156(3):601–10.
[36] Tranchart H, Gaujoux S, Rebours V, et al. Preoperative CT scan helps to predict the occurrence of severe pancreatic Fistula after pancreaticoduodenectomy. Ann Surg 2012;256(1):139–45.
[37] Ridolfi C, Angiolini MR, Gavazzi F, et al. Morphohistological features of pancreatic stump are the main determinant of pancreatic fistula after pancreatoduodenectomy. Biomed Res Int 2014;2014.
[38] Kakizawa N, Noda H, Watanabe F, Ichida K, Suzuki K, Rikiyama T. A high abdominal aortic calcification score on CT is a risk factor for postoperative pancreatic Fistula in elderly patients undergoing pancreaticoduodenectomy. World J Surg 2018;42(4):1129–37.
[39] Wellner UF, Kayser G, Lapshyn H, et al. A simple scoring system based on clinical factors related to pancreatic texture predicts postoperative pancreatic Fistula preoperatively. HPB (Oxford) 2010;12(10):696–702.
[40] Halle-Smith JM, Vinuela E, Brown RM, et al. A comparative study of risk factors for pancreatic fistula after pancreatoduodenectomy or distal pancreatectomy. HPB (Oxford) 2017;19(8):727–34.
[41] Zhang W, Cai W, He B, Xiang N, Fang C, Jia F. A radiomics-based formula for the preoperative prediction of postoperative pancreatic fistula in patients with pancreaticoduodenectomy. Cancer Manag Res 2018;10:6469–78.
[42] Zarzavadjian Le Bian A, Fuks D, Montali F, et al. Predicting the severity of pancreatic Fistula after pancreaticoduodenectomy: overweight and blood loss as independent risk factors: retrospective analysis of 277 patients. Surg Infect (Larchmt) 2019;20(6):486–91.
[43] McMillan MT, Malleo G, Bassi C, et al. Pancreatic fistula risk for pancreatoduodenectomy: an international survey of surgeon perception. HPB (Oxford) 2017;19(6):515–24.
[44] McMillan MT, Malleo G, Bassi C, et al. Multicenter, prospective trial of selective drain management for pancreatoduodenectomy using risk stratification. Ann Surg 2017;265(6):1209–18.
[45] Witzigmann H, Diener MK, Kienkotter S, et al. No need for routine drainage after pancreatic head resection: the dual-center, randomized, controlled PANDRA trial (ISRCTN04937707). Ann Surg 2016;264(3):528–37.
[46] Goyert N, Eeson G, Kagedan DJ, et al. Pasireotide for the prevention of pancreatic Fistula following pancreaticoduodenectomy: a cost-effectiveness analysis. Ann Surg 2017;265(1):2–10.
[47] Cheng Y, Briarava M, Lai M, et al. Pancreaticojejunostomy versus pancreaticogastrostomy reconstruction for the prevention of postoperative pancreatic fistula following pancreaticoduodenectomy. Cochr Datab Syst Rev 2017;9:CD012257.
[48] Harris AG. Somatostatin and somatostatin analogues: pharmacokinetics and pharmacodynamic effects. Gut 1994;35(3 Suppl):S1–4.
[49] Jang JY, Chang YR, Kim SW, et al. Randomized multicentre trial comparing external and internal pancreatic stenting during pancreaticoduodenectomy. Br J Surg 2016;103(6):668–75.